Misery perfusion and amyloid deposition in atherosclerotic major cerebral artery disease

Hiroshi Yamauchi[a,*], Shinya Kagawa[a], Masaaki Takahashi[a], Naoya Oishi[b], Masahiro Ono[c], Tatsuya Higashi[a,d]

[a] Division of PET Imaging, Shiga Medical Centre Research Institute, Moriyama, Japan
[b] Human Brain Research Center, Graduate School of Medicine, Kyoto University, Kyoto, Japan
[c] Department of Patho-Functional Bioanalysis, Graduate School of Pharmaceutical Sciences, Kyoto University, Kyoto, Japan
[d] National Institute of Radiological Sciences, National Institutes of Quantum and Radiological Science and Technology, Chiba, Japan

A B S T R A C T

Although experimental studies have shown that global cerebral hypoperfusion leads to amyloid deposition in the hemisphere with carotid artery occlusion in rodents, the results of such occurrence are controversial in humans. Hence, we aim to determine whether global cerebral hypoperfusion leading to decreased blood flow relative to metabolic demand [increased oxygen extraction fraction (OEF), misery perfusion] is associated with increases in amyloid deposition in the hemisphere with atherosclerotic major cerebral artery disease in patients. We evaluated the distribution of β-amyloid plaques using positron emission tomography and a [18F]-pyridylbenzofuran derivative (^{18}F-FPYBF-2) in 13 patients with unilateral atherosclerotic disease of the internal carotid artery (ICA) or middle cerebral artery (MCA) disease and no cortical infarction. The distribution volume ratio (DVR) of ^{18}F-FPYBF-2 was calculated using dynamic data and Logan graphical analysis with reference tissue and was correlated with the cerebral blood flow (CBF), cerebral metabolic rate of oxygen ($CMRO_2$), and OEF, obtained from ^{15}O-gas PET. The mean cortical value was calculated as the mean value within the frontal, posterior cingulate, precuneus, parietal, and lateral temporal cortical regions. Significant reductions in CBF and $CMRO_2$ and increases in OEF were found in the hemisphere ipsilateral to the arterial lesion compared with the contralateral hemisphere. There was no significant difference for ^{18}F-FPYBF-2 DVR between hemispheres. The ipsilateral to contralateral ratio of the ^{18}F-FPYBF-2 DVR was increased in 3 patients, while the ipsilateral to contralateral OEF ratio was increased in 4 patients. The incidence of an increased hemispheric DVR ratio was significantly higher in patients with an increased hemispheric OEF ratio (3/4) than in patients without (0/9) ($p < 0.02$). Although the ^{18}F-FPYBF-2 DVR in the ipsilateral hemisphere was positively correlated with OEF after adjustment for the ^{18}F-FPYBF-2 DVR in the contralateral hemisphere using multiple regression analysis ($p < 0.05$), the contribution rate of OEF was small ($R^2 = 5.5\%$). Only one of the 4 patients with an increased hemispheric OEF ratio showed amyloid positivity based on the DVR value. In atherosclerotic major cerebral artery disease, misery perfusion accompanied only small increases of amyloid deposition at best. Misery perfusion was not associated with amyloid positivity.

1. Introduction

Epidemiological studies have shown that risk factors for cerebrovascular disease (CVD) increase the risk of developing Alzheimer's disease (AD).(Breteler, 2000; Gupta and Iadecola, 2015) Several studies have suggested a potential interaction between CVD and amyloid plaque formation, a core pathological features of AD. (Gupta and Iadecola, 2015; Liu et al., 2015) Postmortem studies in patients with AD have reported pronounced atherosclerosis in the circle of Willis,

(Yarchoan et al., 2012) suggesting the presence of cerebral hypoperfusion. The cerebral hypoperfusion due to athero- or arteriosclerosis of the cerebral arteries may be one of the factors contributing to the accelerated deposition of beta amyloid (Aβ) in the brain parenchyma or vasculature, through either increased production or decreased clearance.(Gupta and Iadecola, 2015)

Experimental studies in vitro have shown that hypoxia and/or ischemia promote the cleavage of Aβ from the amyloid precursor protein by up-regulating β-secretase expression and activity.(Iadecola,

2010; Zhang et al., 2007; Zlokovic, 2011) An increase in amyloid deposition in the brain parenchyma or vasculature has been shown in rodent models of global cerebral hypoperfusion following carotid artery occlusion. (Kitaguchi et al., 2009; Okamoto et al., 2012; Zhiyou et al., 2009) Furthermore, reduced flow in the area distal to the atherosclerotic narrowing of the cerebral arteries could impair the vigorous blood flow needed to efficiently clear Aβ via the perivascular routes. (Gupta and Iadecola, 2015) However, the association between cerebral hypoperfusion and amyloid deposition in humans is controversial. Better understanding of this issue is clinically important because the optimal management of vascular risk factors can prevent chronic cerebral hypoperfusion,(Yamauchi et al., 2018) which may delay progression of AD. (Gottesman et al., 2017; Larson et al., 2013)

Positron emission tomography (PET) can reveal amyloid plaque distribution in patients with ischemic stroke.(Liu et al., 2015) Studies on the effect of cerebral hypoperfusion and the presence of carotid artery disease on amyloid deposition have yielded conflicting results. (Hansson et al., 2018; Huang et al., 2012; Sahathevan et al., 2016) One earlier study showed increased amyloid deposition in the hemisphere distal to carotid stenosis (Huang et al., 2012), while another 2 studies did not. (Hansson et al., 2018; Sahathevan et al., 2016) Furthermore, one of the negative studies showed no association between local amyloid deposition and local hypoperfusion in comparisons using perfusion imaging. (Hansson et al., 2018) The reason for the controversial findings might be that the presence of carotid artery disease does not necessarily translate into global cerebral hypoperfusion leading to decreased blood flow relative to metabolic demand [increased oxygen extraction fraction (OEF), misery perfusion], (Baron et al., 1981; Powers, 1991) which may be essential for increased Aβ production. In many patients, collateral perfusion or autoregulatory vasodilation can compensate for the reduction in perfusion pressure due to artery disease. Furthermore, the development of cerebral infarction or selective neuronal damage (Baron et al., 2014; Yamauchi et al., 2007) may decrease the metabolic demand in the brain. Thus, in most stroke patients with carotid artery disease, reduction in CBF may be accompanied by a decrease in the cerebral metabolic rate of oxygen ($CMRO_2$) without increasing OEF (matched low perfusion).(Powers, 1991; Yamauchi et al., 2012) Global increases in OEF (misery perfusion) may be essential in the accelerated deposition of Aβ in the brain through either increased production or decreased clearance.(Gupta and Iadecola, 2015) Lastly, cerebral hypoperfusion may affect the distribution of the PET amyloid ligand by changing delivery and clearance to and from brain tissue. (van Berckel et al., 2013) However, quantitative evaluation of amyloid deposition was not performed in previous studies. To address this issue, hemodynamic and metabolic parameters as well as amyloid deposition should be directly measured, and to the best of our knowledge, no studies have investigated the association between global misery perfusion and amyloid deposition in patients with major cerebral artery disease, using quantitative measurements of these parameters with PET. Hence, in this study we aim to determine whether global cerebral hypoperfusion leading to decreased blood flow relative to metabolic demand (increased OEF, misery perfusion) is associated with increases in amyloid deposition in the hemisphere with atherosclerotic internal carotid artery (ICA) or middle cerebral artery (MCA) disease.

2. Materials and methods

2.1. Patients

We recruited 13 consecutive patients with unilateral atherosclerotic occlusion or stenosis of the ICA or MCA (Table 1). They were referred to our PET unit over a period of 12 months to undergo hemodynamic evaluation as part of a clinical assessment to determine the need for vascular reconstructive surgery. Inclusion criteria were: (1) occlusion or stenosis of the extracranial ICA (> 60% diameter reduction according

Table 1
Patient characteristics.

Characteristic	
No. of patients	13
Age, years (mean ± SD)	69 ± 8
Sex	
Male, n	9
Female, n	4
Symptomatic, n	11
Cerebral infarction, n	11
Qualifying artery, n	
ICA (occlusion/stenosis)	9 (5/4)
MCA (occlusion/stenosis)	4 (3/1)
Comorbidities, n	
Hypertension	8
Diabetes mellitus	3
Ischemic heart disease	0
Hypercholesterolemia	4
Smoking habit (current and former), n	5

ICA, internal carotid artery; SD, standard deviation.

to the North American Symptomatic Carotid Endarterectomy Trial criteria (North American Symptomatic Carotid Endarterectomy Trial Collaborators., 1991)) or intracranial ICA or MCA (> 50% diameter reduction according to the WASID criteria (Samuels et al., 2000)) as documented by conventional or magnetic resonance angiography; (2) functional independence in daily life (a modified Rankin Scale score < 3); and (3) for symptomatic patients, history of transient ischemic attack (TIA) or minor completed stroke in the ICA or MCA distributions. The exclusion criteria were: (1) infarction in the cerebral cortex ipsilateral or contralateral to the arterial lesion or infarction in the cerebellum detectable on routine MRI images (T1-weighted, T2-weighted, or fluid-attenuated inversion recovery images); (2) history of TIA or stroke in regions other than the relevant ICA or MCA territory; (3) history of vascular reconstructive surgery; (4) contralateral ICA or MCA stenosis (> 50%), (5) presence of potential sources of cardiogenic embolism; or (6) major psychiatric or neurological disease other than TIA or stroke.

The patients included 9 men and 4 women aged 47–83 years (mean ± standard deviation: 69 ± 8 years) (Table 1). Of the 13 patients enrolled, 2 were asymptomatic, 3 experienced TIA, and 8 had completed stroke. The interval between the diagnosis of artery diseases and PET evaluation was 3.2 ± 3.9 months (range, 0.4–13.4 months). The interval between the stroke event and PET evaluation in symptomatic patients was 3.2 ± 2.9 months (range, 0.4–10 months). The qualifying artery occlusion type was extracranial ICA occlusion in 3 cases, extracranial ICA stenosis in 4, intracranial ICA occlusion in 2, MCA occlusion in 3, and MCA stenosis in 1. MRI revealed internal border zone infarction in 3 cases, superficial perforator infarction in 6, and deep perforator infarction in 2. No patients complained of episodic memory impairment.

All protocols in this study were approved by the Shiga General Hospital Institutional Review Board, the Human Study Committee (number 99). All participants provided written informed consent. All experiments were performed in accordance with the Declaration of Helsinki and Good Clinical Practice.

2.2. PET measurements

We performed PET scans using a whole-body scanner (GE Advance; General Electric Medical System, Wauwatosa, WI), which permits simultaneous acquisition of 35 image slices with inter-slice spacing of 4.25 mm.(Okazawa et al., 2001) Performance tests showed the intrinsic resolution of the scanner to be 4.6 to 5.7 mm in the transaxial direction and 4.0 to 5.3 mm in the axial direction. A transmission scan was

performed using ^{68}Ge/^{68}Ga for attenuation correction in each patient before administration of the tracer. During reconstruction of the PET data using filtered back projection, images were blurred to 8.5 mm of the full width at the half maximum in the transaxial direction using a Hanning filter. Functional images were reconstructed as 128×128 pixels, with each pixel representing an area of 2.0×2.0 mm.

First, a series of ^{15}O-gas experiments was performed.(Okazawa et al., 2001) A small cannula was placed in the left brachial artery for blood sampling. The participants continuously inhaled C^{15}O$_2$ and ^{15}O$_2$ through a mask. The scan time was 5 min. Bolus inhalation of C^{15}O with scanning for 3 min was used to measure the CBV. Arterial samples were manually obtained during the scanning. The radioactivity of the radiotracer, oxygen content, and hematocrit were also measured.

We developed a benzofuran derivative for the imaging of Aβ plaques, 5-(5-(2-(2-(2-[18F]fluoroethoxy)ethoxy)ethoxy)benzofuran-2-yl)-N-methylpyridin-2-amine ([18F]FPYBF-2).(Ono et al., 2011) Following the ^{15}O-gas experiment, an ^{18}F- FPYBF-2 evaluation was performed. (Higashi et al., 2018; Nishii et al., 2018) ^{18}F-FPYBF-2 was prepared in-house. The ^{18}F-fluoride was produced with a cyclotron (CYPRIS HM18; Sumitomo Heavy Industries Ltd., Tokyo, Japan) by the ^{18}O(p,n)^{18}F reaction on 98% enriched ^{18}O water. The radiosynthesis of ^{18}F-FPYBF-2 was performed using a modification of the methods described by Ono et al. (Ono et al., 2011) on a hybrid, cassette-type multipurpose automatic synthesizer module (JFE Engineering Corporation, Tokyo, Japan). The fluorination of the mesylate precursor occurred in dimethyl sulfoxide in the presence of Kryptofix 2.2.2 and potassium carbonate. The mixture was then treated with aqueous hydrochloric acid. After purification of the crude product by high-performance liquid chromatography, ^{18}F- FPYBF-2 was eluted with 2.5% ethanol in saline. Specific activities at the time of injection were 338.7 ± 50.9 GBq/μmol. Patients received approximately 200 MBq of ^{18}F- FPYBF-2 by slow intravenous injection into the right antecubital vein. A 70-min dynamic PET scan was started at the time of tracer administration with frame durations of $10\,s \times 6$, $15\,s \times 8$, $30\,s \times 4$, $60\,s \times 5$, $5\,min \times 4$, and $10\,min \times 4$.

We calculated the CBF, CMRO$_2$, and OEF using the steady-state method.(Frackowiak et al., 1980; Okazawa et al., 2001) The CMRO$_2$ and OEF were corrected according to the CBV.(Lammertsma and Jones, 1983)

The standardized uptake value (SUV) for ^{18}F- FPYBF-2 was calculated as follows: SUV = C (kBq/ml)/ID (kBq)/body weight (g); where C represents the tissue activity concentration measured by PET, and ID represents the injected dose.

The distribution volume ratio (DVR) of ^{18}F- FPYBF-2 was calculated using dynamic data and Logan graphical analysis with reference tissue, with the cerebellar cortex as the reference region. (Logan et al., 1996; Lopresti et al., 2005) In patients with ICA or MCA disease, the cerebellar cortex ipsilateral to the arterial disease was used as the reference region because the effect of cerebellar deafferentation was unclear. We selected one tomographic plane corresponding to the level of the cerebellar cortex and pons obtained from the early phase of dynamic PET data. We manually placed an irregular region of interest (ROI) in the cerebellar cortex. The ROI was transferred to the dynamic PET data for the calculation of DVR.

2.3. Data analysis

For ^{18}F- FPYBF-2 PET scanning analysis, in-house PET template construction was performed for ^{18}F-FPYBF-2 PET.(Ashburner and Friston, 1999; Higashi et al., 2018; Kudo et al., 2007) In addition to the DVR value, the standardized uptake value ratio (SUVR) of each region, indicating amyloid deposition, was calculated as follows: SUVR = SUV brain / SUV cerebellar cortex, where SUV brain and SUV cerebellar cortex indicate the SUV in each brain region and the cerebellar cortex, respectively, since the cerebellar cortex can be used as a reference brain region that lacks amyloid plaque.(Kudo et al., 2007; Price et al., 2005)

To obtain quantitative regional DVR or SUVR values of ^{18}F-FPYBF-2 PET, we performed automated ROI analyses. The automated anatomical labeling atlas (AAL),(Tzourio-Mazoyer et al., 2002) which is publicly and widely available from the Internet (MRIcro/MRIcron, http://www.mricro.com/), was used for template-based predefined ROIs. The AAL atlas consists of 45 anatomical ROIs in each hemisphere and a cerebellar parcellation with 26 ROIs.(Schmahmann et al., 1999) The AAL ROIs were finally masked with the gray matter defined by the MNI152 standard-space T1-weighted average structural template image available from the FSL software (http://www.fmrib.ox.ac.uk/fsl) and used as the predefined ROIs.

The reconstructed ^{18}F-FPYBF-2 PET images were spatially normalized to a standard Montreal Neurologic Institute (MNI) space using the discrete cosine transform-based approach(Ashburner and Friston, 1999) implemented in SPM8 (Wellcome Trust Centre for Neuroimaging, University College London, UK) with the in-house ^{18}F-FPYBF-2 PET template. All AAL ROIs in the standard MNI space were inversely transformed to individual spaces by SPM8 using the inverse deformation field. Since these individual ROIs are automatically defined, operator-introduced bias when defining ROIs manually can be avoided. (Oishi et al., 2007) The cerebellar parcellations were combined and used as reference regions to create SUVR images. In patients with ICA or MCA disease, the value of SUV in the cerebellar cortex ipsilateral to the arterial disease was used because the effect of cerebellar deafferentation on ^{18}F-FPYBF-2 SUV was unclear. Mean DVR or SUVR values within 90 anatomical ROIs in both hemispheres were calculated by an in-house Matlab script.

Finally, as a representative value for cortical amyloid plaque deposition of each subject, the mean cortical index (MCI) was defined as the mean DVR or SUVR value within the frontal, posterior cingulate, precuneus, parietal, and lateral temporal cortical regions (Higashi et al., 2018; Mormino et al., 2008) The MCI values were calculated as the average of the values of all those ROIs, weighted by region size. According to our previous study in normal subjects and patients with Alzheimer's disease, a mean SUVR value above 1.20 was considered amyloid positive. (Higashi et al., 2018)

The mean $\pm$ SD value of the left to right or the right to left ratio of ^{18}F- FPYBF-2 MCI (DVR) in the 10 normal controls (4 men and 6 women), aged 57 ± 11 (mean $\pm$ SD) years was 1.007 ± 0.016 and 0.993 ± 0.016, respectively. No subjects showed a mean SUVR value above 1.20 (amyloid positive). In patients, increase of the relative ^{18}F-FPYBF-2 DVR beyond the upper 95% limit (the mean plus $_9t_{0.05}$SD) defined in normal subjects (above 1.042 for patients with left arterial disease and above 1.028 for patients with right arterial disease) was considered to be an increased hemispheric DVR ratio, while decrease of the relative ^{18}F- FPYBF-2 DVR beyond the lower 95% limit (the mean minus $_9t_{0.05}$SD) defined in normal subjects (below 0.971 for left disease and 0.958 for right) was considered to be a decreased hemispheric DVR ratio. The distributions are not left-right symmetrical, which may be related to widespread asymmetries at both hemispheric and regional levels, with a generally thicker cortex but smaller surface area in the left hemisphere relative to the right. (Kong et al., 2018)

For the ^{15}O gas PET scanning analysis, we employed the same automated ROI analysis using AAL ROIs. The mean hemispheric values within the frontal, posterior cingulate, precuneus, parietal, and lateral temporal cortical regions were calculated in the hemisphere ipsilateral or contralateral to the ICA or MCA disease. The mean $\pm$ SD value of the left to right or the right to left ratio of OEF in the 7 normal controls (4 men and 3 women), aged 47 ± 7 (mean $\pm$ SD) years was 1.010 ± 0.018 and 0.991 ± 0.018, respectively. In patients, increase of the relative OEF beyond the upper 95% limit (the mean plus $_6t_{0.05}$SD) defined in normal subjects (above 1.054 for patients with left arterial disease and above 1.034 for patients with right arterial disease) was considered to be an increased hemispheric OEF ratio, while decrease of the relative OEF beyond the lower 95% limit (the mean minus $_6t_{0.05}$SD) defined in normal subjects (below 0.965 for left disease and 0.946 for

Table 2
Positron emission tomography values in the hemisphere ipsilateral and contralateral to the diseased artery.

	Hemisphere	
Variable	Ipsilateral	Contralateral
CBF (ml/100 g/min)	30.7 ± 5.2**	33.9 ± 4.6
CMRO$_2$ (ml/100 g/min)	2.91 ± 0.67*	3.06 ± 0.63
OEF (%)	54.2 ± 10.1**	51.7 ± 9.8
CBV (ml/100 g)	4.23 ± 0.70	3.98 ± 0.62
^{18}F-FPYBF-2 (DVR)	0.88 ± 0.10	0.89 ± 0.11

Values are reported as mean ± standard deviation.
CMRO$_2$, cerebral metabolic rate of oxygen; OEF, oxygen extraction fraction; DVR, distribution volume ratio.
*$P < 0.05$, and **$P < 0.01$ vs. corresponding value in the contralateral hemisphere (Wilcoxon signed-rank-tests).
Normal values for CBF, CMRO2, OEF, and CBV in the 7 controls were 44.6 ± 4.5, 3.43 ± 0.33, 44.5 ± 3.8, and 3.98 ± 0.48, respectively.

right) was considered to be a decreased hemispheric OEF ratio.

2.4. Statistical analysis

The statistical analysis was performed using StatView™ (SAS Institute Inc., Cary, NC, USA). PET variable values between 2 groups were compared using Mann-Whitney U tests or Wilcoxon signed-rank-tests, as appropriate. The relationships between 2 variables were analyzed using Spearman correlation analyses or Fisher's exact tests, as appropriate. A multiple regression model was used to analyze the relationship between the OEF and the ^{18}F- FPYBF-2 DVR in the ipsilateral hemisphere after adjustment for the ^{18}F- FPYBF-2 DVR in the contralateral hemisphere. For all analyses, statistical significance was set at $p < 0.05$.

3. Results

Significant decreases in CBF and CMRO$_2$ along with increases in OEF were found in the hemisphere ipsilateral to the arterial lesion compared with the contralateral hemisphere (Table 2). There was no significant difference for ^{18}F-FPYBF-2 DVR between hemispheres. However, the ipsilateral to contralateral ratio of ^{18}F- FPYBF-2 DVR varied among patients and was beyond the upper 95% limit defined in normal subjects in 3 patients. In a Spearman correlation analysis, the ipsilateral to contralateral ^{18}F- FPYBF-2 DVR ratio was tended to be positively correlated with the ipsilateral to contralateral OEF ratio, without statistical significance. (ρ=0.527; $p = 0.067$) (Figs. 1 and 2). The ipsilateral to contralateral OEF ratio was beyond the upper 95% limit defined in normal subjects in 4 patients. The incidence of an increased hemispheric ^{18}F-FPYBF-2 DVR ratio was significantly higher in patients with an increased hemispheric OEF ratio (3/4) than in patients without (0/9) ($p < 0.02$, Fisher's exact test). The hemispheric ^{18}F-FPYBF-2 DVR ratio was higher in patients with an increased hemispheric OEF ratio than in patients without (1.037 ± 0.019 vs. 0.957 ± 0.037; $p < 0.01$, Mann-Whitney U test).

The ^{18}F- FPYBF-2 DVR in the ipsilateral hemisphere was not significantly correlated with CBF, CMRO2, OEF, or CBV values in the ipsilateral hemisphere (Fig. 3), while it was significantly and positively correlated with the ^{18}F- FPYBF-2 DVR in the contralateral hemisphere. After adjustment for the ^{18}F- FPYBF-2 DVR in the contralateral hemisphere using multiple linear regression analysis, the ^{18}F- FPYBF-2 DVR in the ipsilateral hemisphere was significantly and positively correlated with OEF in the ipsilateral hemisphere (Table 3): the^{18}F- FPYBF-2 DVR in the ipsilateral hemisphere = 0.914 FPYBF-2 DVR in the contralateral hemisphere +0.002 OEF (%) - 0.075 (a correlation coefficient of 0.95; $R^2 = 89.7\%$, $p < 0.001$). In this model, the ^{18}F- FPYBF-2 DVR in the contralateral hemisphere and OEF accounted for 84.2% and 5.5%,

respectively, of the variance in ^{18}F- FPYBF-2 DVR in the ipsilateral hemisphere.

There was no correlation between ^{18}F- FPYBF-2 DVR value and the time elapsed from symptoms in 11 symptomatic patients or from diagnosis of artery diseases in 13 patients.

According to the mean cortical SUVR value, 2 patients were amyloid positive (SUVR > 1.20 in the contralateral hemisphere) (Fig. 3). These patients showed the first and second highest mean cortical DVR values in the hemisphere contralateral to the arterial disease. In the hemisphere contralateral to disease, the mean cortical DVR value was significantly correlated with the mean cortical SUVR value; DVR = 0.672 SUVR + 0.153, $r = 0.87$, $p < 0.001$. SUVR > 1.20 corresponded to DVR > 0.96. Three patients showed DVR > 0.96 (amyloid positivity) in the ipsilateral hemisphere, and one of these 3 patients had an increased hemispheric OEF ratio without an increased hemispheric DVR ratio. No patients with an increased hemispheric DVR ratio considered amyloid positive (Fig. 3).

Upper row: an increase of relative FPYBF-2 distribution volume ratio (DVR) (ipsilateral-to-contralateral FPYBF-2 DVR ratio) 1.04, (ipsilateral/contralateral DVR 0.81/0.77), with decreased CBF and increased oxygen extraction fraction (OEF) (ipsilateral/contralateral ratio 1.29; 63/48%), despite reduction in cerebral metabolic rate of oxygen (CMRO$_2$), in a patient with right (R) internal carotid artery occlusion.

Lower row: a reduction in relative FPYBF-2 DVR (0.91, 0.91/1.0) in a patient with left (L) middle cerebral artery occlusion with decreases of both CBF and CMRO$_2$, and normal OEF (1.01; 49/48%).

4. Discussion

Our study revealed that global cerebral hypoperfusion leading to decreased blood flow relative to metabolic demand (increases in OEF; misery perfusion) was associated with only a slight increase in amyloid deposition in the hemisphere with atherosclerotic ICA or MCA disease. In the hemisphere ipsilateral to the arterial lesion with reduction in CBF and CMRO$_2$, and elevation of OEF, ^{18}F- FPYBF-2 DVR was unchanged compared with the contralateral hemisphere. The ipsilateral-to-contralateral ratio of the ^{18}F- FPYBF-2 DVR, which may reflect the independent effect of ICA or MCA disease on the change, varied among patients and was positively correlated with the ipsilateral-to-contralateral ratio of the OEF, which suggested that misery perfusion defined as an increased hemispheric OEF ratio was associated with increased amyloid deposition defined as an increased hemispheric ^{18}F-FPYBF-2 DVR ratio. Furthermore, after adjustment for the ^{18}F- FPYBF-2 DVR in the contralateral hemisphere, which may reflect the effect of the other factors contributing to amyloid deposition, OEF was positively correlated with the ^{18}F- FPYBF-2 DVR in the ipsilateral hemisphere. Therefore, misery perfusion could potentially be associated with an increase in amyloid deposition. Some clinical studies in patients with cardiac arrest or after cardiac surgery have shown that hypoxia acutely increases Aβ levels in the blood or cerebrospinal fluid.(Reinsfelt et al., 2013; Mortberg et al., 2011)

However, we also observed that an increased hemispheric ^{18}F-FPYBF-2 DVR ratio (ipsilateral to contralateral ratio) was found in only 3/13 patients, and the magnitude of these changes was very small. No patients with an increased hemispheric DVR ratio considered amyloid positive based on the DVR values in the ipsilateral hemisphere. In the multiple regression model produced, 20% increases of OEF values resulted in increases of DVR values by 0.04 only, and the value of R^2 for OEF was very small (5.5%). Therefore, misery perfusion had only a slight effect on amyloid deposition at best and was not associated with amyloid positivity.

There are three published studies on amyloid deposition in humans in relation to hypoperfusion. (Hansson et al., 2018; Huang et al., 2012; Sahathevan et al., 2016) All of these studies did not perform quantitative evaluation of amyloid deposition using dynamic scanning. Therefore, the results might be contaminated by flow artifacts
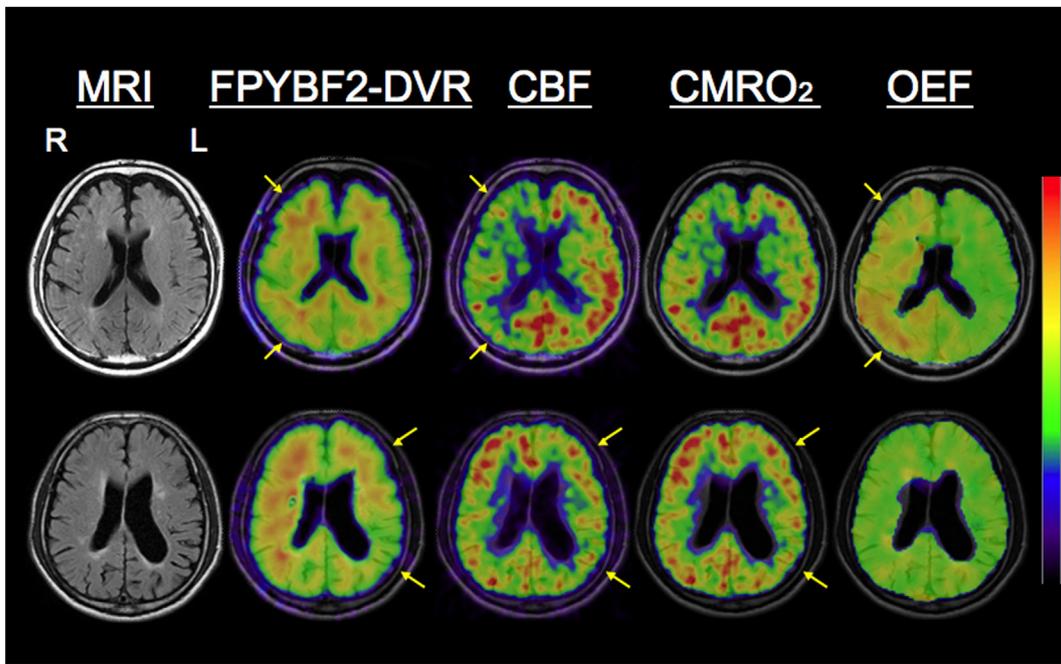
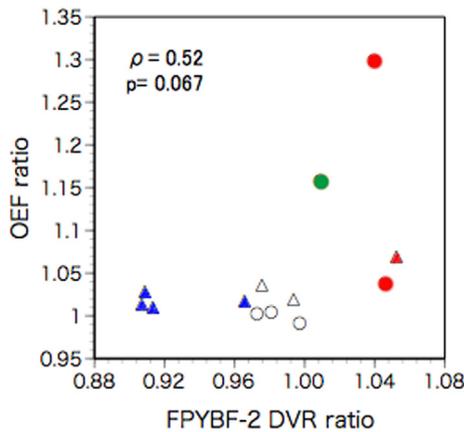**Fig. 1.** Representative positron emission tomography images.

Fig. 2. Scatter diagram plotting the ipsilateral-to-contralateral ratio of ^{18}F-FPYBF-2 distribution volume ratio (DVR) against the ipsilateral-to-contralateral ratio of oxygen extraction fraction (OEF). Triangles indicate patients with left artery diseases and circles indicate patients with right artery diseases. Red symbols indicate patients with an increased OEF ratio and an increased DVR ratio, a green symbol indicates a patient with an increased OEF ratio and a normal DVR ratio, blue symbols indicates patients with a normal OEF ratio and a decreased DVR ratio, white symbols indicate patients with a normal OEF ratio and a normal DVR ratio. (For interpretation of the references to color in this figure legend, the reader is referred to the web version of this article.)

(decreased tracer uptake due to reduced delivery). (van Berckel et al., 2013) The small change in the present study was consistent with a previous study that reported increased amyloid deposition in demented patients with ICA stenosis, as compared with elderly controls.(Huang et al., 2012) However, the effect of the stenosis on cerebral perfusion was unclear. In such patients, the duration of misery perfusion, as indicated by increased OEF, is unclear. Misery perfusion might contribute to amyloid positivity, but the effect might be very small in the short-term and might only become more apparent during long-term follow-up. In our patients, the interval between the diagnosis of artery diseases and PET evaluation was 3.2 ± 3.9 months (range, 0.4–13.4 months). The slight effect during one year around might accumulate over > 10 years, leading to amyloid positivity. The two previous studies with
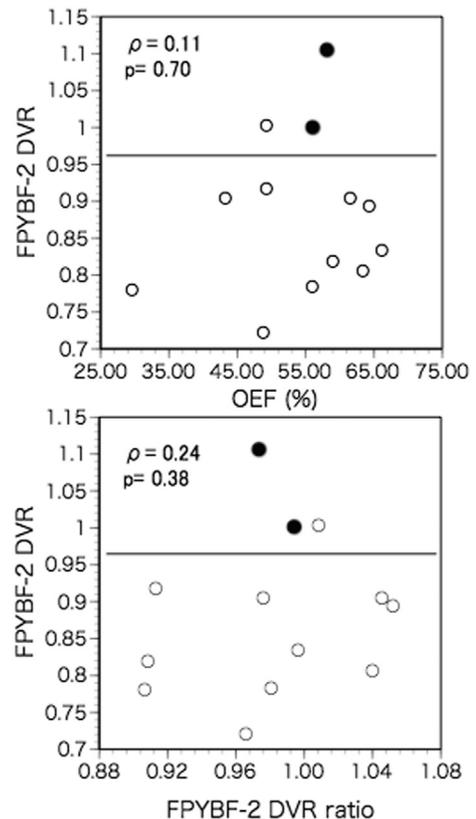

Fig. 3. Scatter diagram plotting the ipsilateral [18]F- FPYBF-2 distribution volume ratio (DVR) against the values for oxygen extraction fraction (OEF) in the ipsilateral hemisphere (upper), and against the ipsilateral-to-contralateral ratio of [18]F- FPYBF-2 DVR (lower). Closed circles indicate amyloid-positive patients with SUVR > 1.20 in the contralateral hemisphere. Lines indicate a cut off value of DVR for amyloid positivity (> 0.96).

negative results also had a mean occlusion time of 22 months and a follow-up time of 18 months. (Hansson et al., 2018; Huang et al., 2012; Sahathevan et al., 2016) Late-life brain amyloid deposition is reported

Table 3

Multiple linear regression analysis with the[18]F- FPYBF-2 DVR in the ipsilateral hemisphere as dependent variable.

Independent variable	Coefficient	Standard error	Standard coefficient	t	P-value
Ipsilateral OEF (%)	0.002	0.001	0.234	2.292	< 0.05
Contralateral ^{18}F-FPYBF-2 (DVR)	0.914	0.1	0.938	9.188	< 0.0001

OEF, oxygen extraction fraction; DVR, distribution volume ratio.

to be associated with midlife vascular risk factors, not with late-life vascular risk factors.(Gottesman et al., 2017) Alternatively, misery perfusion may have pathogenic significance when combined with other factors leading to increased Aβ production or decreased Aβ clearance, as shown in *APP*-overexpressing mouse models.(Kitaguchi et al., 2009) Further studies in more patients with misery perfusion are needed to test these hypotheses.

Overall, the value of [18]F- FPYBF-2 DVR was unchanged, which may reflect that only a few patients had misery perfusion (an increased hemispheric OEF ratio). The mechanism underlying the decreased ^{18}F-FPYBF-2 DVR in patients without misery perfusion is unclear. We used dynamic scanning protocols and quantitative data analysis methods. Therefore, it seems unlikely that a decreased delivery of the radiotracer due to a decreased blood flow caused the decreased [18]F- FPYBF-2 DVR. (van Berckel et al., 2013) Significant decreases in $CMRO_2$ was found in the hemisphere ipsilateral to the arterial lesion compared with the contralateral hemisphere. In patients with ICA or MCA disease, misery perfusion may cause selective cortical neuronal damage, which may be accompanied by decreases in $CMRO_2$. (Baron et al., 2014; Yamauchi et al., 2007) The low [18]F- FPYBF-2 DVR in the normal-appearing cortical regions with decreased $CMRO_2$ suggests that irreversible tissue damage, including selective neuronal damage, might decrease amyloid deposition in the cerebral cortex. Insoluble Aβ deposition may be disassembled by the inflammation caused by cerebral ischemia, because incomplete infarction may lead to microglial activation (Thiel et al., 2014) and subsequent amyloid clearance, resulting in a reduction in amyloid deposition and decreased metabolism.(Akiyama and McGeer, 2004; Yamada et al., 2011) Microglia reportedly accumulates in amyloid plaques in AD patients and effectively clears Aβ through phagocytosis and proteolysis.(Heneka et al., 2015) A study of the postmortem AD brain showed that in area with incomplete infarction, amyloid deposits were absent in the presence of a high concentration of activated microglia, while adjacent areas had abundant amyloid deposits. (Akiyama and McGeer, 2004) Furthermore, decreased [18]F- FPYBF-2 DVR in the region with decreased $CMRO_2$ might reflect reduced neuronal Aβ secretion due to decreased brain activity in the presence of neuronal damage. (Cirrito et al., 2005) Misery perfusion might cause cognitive impairment through ischemic tissue damage with decreases in amyloid deposition in the short term as well as through increases in amyloid deposition in the long term.

We acknowledge that there are some limitations to our study. First, the sample size may have been small and studies with a larger number of patients and longer follow-up periods are needed to confirm our results. However, our cohort included patients with variable degrees of hemodynamic impairment, enabling us to analyze the relationship between misery perfusion and amyloid deposition. Second, we could not correct for partial volume effects. The decrease in cortical FPYBF-2 DVR could at least partly reflect the effect of cortical atrophy and a partial volume effect. This effect might lead to underestimation of FPYBF-2 DVR in the hemisphere with arterial disease and might affect the association between [18]F- FPYBF-2 DVR and OEF.

5. Conclusions

In atherosclerotic ICA or MCA disease, global cerebral hypoperfusion leading to increases in OEF (misery perfusion) accompanied only small increases of amyloid deposition. Then, misery perfusion was not

associated with amyloid positivity. It appears that if there are increases in amyloid deposition along with misery perfusion, they are very small at best. The findings in the present study did not strongly support our hypothesis, and in turn more affected patients should be studied in the future.

Disclosures

None.

References

Akiyama, H., McGeer, P.L., 2004. Specificity of mechanisms for plaque removal after A beta immunotherapy for Alzheimer disease. Nat. Med. 10, 117–118 (author reply 118-119).

Ashburner, J., Friston, K.J., 1999. Nonlinear spatial normalization using basis functions. Hum. Brain Mapp. 7, 254–266.

Baron, J.C., Bousser, M.G., Rey, A., Guillard, A., Comar, D., Castaigne, P., 1981. Reversal of focal "misery-perfusion syndrome" by extra-intracranial arterial bypass in hemodynamic cerebral ischemia. A case study with [15]O positron emission tomography. Stroke 12, 454–459.

Baron, J.C., Yamauchi, H., Fujioka, M., Endres, M., 2014. Selective neuronal loss in ischemic stroke and cerebrovascular disease. J. Cereb. Blood Flow Metab. 34, 2–18.

Breteler, M.M., 2000. Vascular risk factors for Alzheimer's disease: an epidemiologic perspective. Neurobiol. Aging 21, 153–160.

Cirrito, J.R., Yamada, K.A., Finn, M.B., Sloviter, R.S., Bales, K.R., May, P.C., Schoepp, D.D., Paul, S.M., Mennerick, S., Holtzman, D.M., 2005. Synaptic activity regulates interstitial fluid amyloid-beta levels in vivo. Neuron 48, 913–922.

Frackowiak, R.S.J., Lenzi, G.L., Jones, T., Heather, J.D., 1980. Quantitative measurement of regional cerebral blood flow and oxygen metabolism in man using [15]O and positron emission tomography: theory, procedure, and normal values. J. Comput. Assist. Tomogr. 4, 727–736.

Gottesman, R.F., Schneider, A.L., Zhou, Y., Coresh, J., Green, E., Gupta, N., Knopman, D.S., Mintz, A., Rahmim, A., Sharrett, A.R., Wagenknecht, L.E., Wong, D.F., Mosley, T.H., 2017. Association between midlife vascular risk factors and estimated brain amyloid deposition. JAMA 317, 1443–1450.

Gupta, A., Iadecola, C., 2015. Impaired Aβ clearance: a potential link between atherosclerosis and Alzheimer's disease. Front. Aging Neurosci. 7, 115.

Hansson, O., Palmqvist, S., Ljung, H., Cronberg, T., van Westen, D., Smith, R., 2018. Cerebral hypoperfusion is not associated with an increase in amyloid beta pathology in middle-aged or elderly people. Alzheimers Dement. 14, 54–61.

Heneka, M.T., Carson, M.J., El Khoury, J., Landreth, G.E., Brosseron, F., Feinstein, D.L., Jacobs, A.H., Wyss-Coray, T., Vitorica, J., Ransohoff, R.M., Herrup, K., Frautschy, S.A., Finsen, B., Brown, G.C., Verkhratsky, A., Yamanaka, K., Koistinaho, J., Latz, E., Halle, A., Petzold, G.C., Town, T., Morgan, D., Shinohara, M.L., Perry, V.H., Holmes, C., Bazan, N.G., Brooks, D.J., Hunot, S., Joseph, B., Deigendesch, N., Garaschuk, O., Boddeke, E., Dinarello, C.A., Breitner, J.C., Cole, G.M., Golenbock, D.T., Kummer, M.P., 2015. Neuroinflammation in Alzheimer's disease. Lancet Neurol. 14, 388–405.

Higashi, T., Nishii, R., Kagawa, S., Kishibe, Y., Takahashi, M., Okina, T., Suzuki, N., Hasegawa, H., Nagahama, Y., Ishizu, K., Oishi, N., Kimura, H., Watanabe, H., Ono, M., Saji, H., Yamauchi, H., 2018. Ann. Nucl. Med. 2018, 206–216 (18)F-FPYBF-2, a new F-18-labelled amyloid imaging PET tracer: first experience in 61 volunteers and 55 patients with dementia.

Huang, K.L., Lin, K.J., Ho, M.Y., Chang, Y.J., Chang, C.H., Wey, S.P., Hsieh, C.J., Yen, T.C., Hsiao, I.T., Lee, T.H., 2012. Amyloid deposition after cerebral hypoperfusion: evidenced on [(18)F]AV-45 positron emission tomography. J. Neurol. Sci. 319, 124–129.

Iadecola, C., 2010. The overlap between neurodegenerative and vascular factors in the pathogenesis of dementia. Acta Neuropathol. 120, 287–296.

Kitaguchi, H., Tomimoto, H., Ihara, M., Shibata, M., Uemura, K., Kalaria, R.N., Kihara, T., Asada-Utsugi, M., Kinoshita, A., Takahashi, R., 2009. Chronic cerebral hypoperfusion accelerates amyloid beta deposition in APPSwInd transgenic mice. Brain Res. 1294, 202–210.

Kong, X.Z., Mathias, S.R., Guadalupe, T., Glahn, D.C., Franke, B., Crivello, F., Tzourio-Mazoyer, N., Fisher, S.E., Thompson, P.M., Francks, C., 2018. Mapping cortical brain

asymmetry in 17,141 healthy individuals worldwide via the ENIGMA consortium. Proc. Natl. Acad. Sci. U. S. A. 115, E5154–E5163.

Kudo, Y., Okamura, N., Furumoto, S., Tashiro, M., Furukawa, K., Maruyama, M., Itoh, M., Iwata, R., Yanai, K., Arai, H., 2007. 2-(2-[2-Dimethylaminothiazol-5-yl]ethenyl)-6-(2-[fluoro]ethoxy)benzoxazole: a novel PET agent for in vivo detection of dense amyloid plaques in Alzheimer's disease patients. J. Nucl. Med. 48, 553–561.

Lammertsma, A.A., Jones, T., 1983. Correction for the presence of intravascular oxygen-15 in the steady-state technique for measuring regional oxygen extraction ratio in the brain: 1. Description of the method. J. Cereb. Blood Flow Metab. 3, 416–424.

Larson, E.B., Yaffe, K., Langa, K.M., 2013. New insights into the dementia epidemic. N. Engl. J. Med. 369, 2275–2277.

Liu, W., Wong, A., Law, A.C., Mok, V.C., 2015. Cerebrovascular disease, amyloid plaques, and dementia. Stroke 46, 1402–1407.

Logan, J., Fowler, J.S., Volkow, N.D., Wang, G.J., Ding, Y.S., Alexoff, D.L., 1996. Distribution volume ratios without blood sampling from graphical analysis of PET data. J. Cereb. Blood Flow Metab. 16, 834–840.

Lopresti, B., Klunk, W.E., Mathis, C.A., Hoge, J.A., Ziolko, S.K., Lu, X., Meltzer, C.C., Schimmel, K., Tsopelas, N.D., DeKosky, S.T., Price, J.C., 2005. Simplified quantification of Pittsburgh Compound B amyloid imaging PET studies: a comparative analysis. J. Nucl. Med. 46, 1959–1972.

Mormino, E.C., Kluth, J.T., Madison, C.M., Rabinovici, G.D., Baker, S.L., Miller, B.L., Koeppe, R.A., Mathis, C.A., Weiner, M.W., Jagust, W.J., 2008. Episodic memory loss is related to hippocampal-mediated beta-amyloid deposition in elderly subjects. Brain 132, 1310–1323.

Nishii, R., Higashi, T., Kagawa, S., Okuyama, C., Kishibe, Y., Takahashi, M., Okina, T., Suzuki, N., Hasegawa, H., Nagahama, Y., Ishizu, K., Oishi, N., Kimura, H., Watanabe, H., Ono, M., Saji, H., Yamauchi, H., 2018. (18)F-FPYBF-2, a new F-18 labelled amyloid imaging PET tracer: biodistribution and radiation dosimetry assessment of first-in-man (18)F-FPYBF-2 PET imaging. Ann. Nucl. Med. 32, 256–263.

North American Symptomatic Carotid Endarterectomy Trial Collaborators, 1991. Beneficial effect of carotid endarterectomy in symptomatic patients with high-grade carotid stenosis. N. Engl. J. Med. 325, 445–453.

Oishi, N., Hashikawa, K., Yoshida, H., Ishizu, K., Ueda, M., Kawashima, H., Saji, H., Fukuyama, H., 2007. Quantification of nicotinic acetylcholine receptors in Parkinson's disease with (123)I-5IA SPECT. J. Neurol. Sci. 256, 52–60.

Okamoto, Y., Yamamoto, T., Kalaria, R.N., Senzaki, H., Maki, T., Hase, Y., Kitamura, A., Washida, K., Yamada, M., Ito, H., Tomimoto, H., Takahashi, R., Ihara, M., 2012. Cerebral hypoperfusion accelerates cerebral amyloid angiopathy and promotes cortical microinfarcts. Acta Neuropathol. 123, 381–394.

Okazawa, H., Yamauchi, H., Sugimoto, K., Takahashi, M., Toyoda, H., Kishibe, Y., Shio, H., 2001. Quantitative comparison of the bolus and steady-state methods for measurement of cerebral perfusion and oxygen metabolism: positron emission tomography study using ^{15}O gas and water. J. Cereb. Blood Flow Metab. 21, 793–803.

Ono, M., Cheng, Y., Kimura, H., Cui, M., Kagawa, S., Nishii, R., Saji, H., 2011. Novel 18F-labeled benzofuran derivatives with improved properties for positron emission tomography (PET) imaging of β-amyloid plaques in Alzheimer's brains. J. Med. Chem. 54, 2971–2979.

Powers, W.J., 1991. Cerebral hemodynamics in ischemic cerebrovascular disease. Ann. Neurol. 29, 231–240.

Price, J.C., Klunk, W.E., Lopresti, B.J., Lu, X., Hoge, J.A., Ziolko, S.K., Holt, D.P., Meltzer, C.C., DeKosky, S.T., Mathis, C.A., 2005. Kinetic modeling of amyloid binding in humans using PET imaging and Pittsburgh compound-B. J. Cereb. Blood Flow Metab. 25, 1528–1547.

Reinsfelt, B., Westerlind, A., Blennow, K., Zetterberg, H., Ricksten, S.E., 2013. Open-heart surgery increases cerebrospinal fluid levels of Alzheimer-associated amyloid beta. Acta Anaesthesiol. Scand. 57, 82–88.

Sahathevan, R., Linden, T., Villemagne, V.L., Churilov, L., Ly, J.V., Rowe, C., Donnan, G., Brodtmann, A., 2016. Positron emission tomographic imaging in stroke: cross-sectional and follow-up assessment of amyloid in ischemic stroke. Stroke 47, 113–119.

Samuels, O.B., Joseph, G.J., Lynn, M.J., Smith, H.A., Chimowitz, M.I., 2000. A standardized method for measuring intracranial arterial stenosis. AJNR Am. J. Neuroradiol. 21, 643–646.

Schmahmann, J.D., Doyon, J., McDonald, D., Holmes, C., Lavoie, K., Hurwitz, A.S., Kabani, N., Toga, A., Evans, A., Petrides, M., 1999. Three-dimensional MRI atlas of the human cerebellum in proportional stereotaxic space. Neuroimage 10, 233–260.

Thiel, A., Cechetto, D.F., Heiss, W.D., Hachinski, V., Whitehead, S.N., 2014. Amyloid burden, neuroinflammation, and links to cognitive decline after ischemic stroke. Stroke 45, 2825–2829.

Tzourio-Mazoyer, N., Landeau, B., Papathanassiou, D., Crivello, F., Etard, O., Delcroix, N., Mazoyer, B., Joliot, M., 2002. Automated anatomical labeling of activations in SPM using a macroscopic anatomical parcellation of the MNI MRI single-subject brain. Neuroimage 15, 273–289.

van Berckel, B.N., Ossenkoppele, R., Tolboom, N., Yaqub, M., Foster-Dingley, J.C., Windhorst, A.D., Scheltens, P., Lammertsma, A.A., Boellaard, R., 2013. Longitudinal amyloid imaging using ^{11}C-PiB: methodologic considerations. J. Nucl. Med. 54, 1570–1576.

Yamada, M., Ihara, M., Okamoto, Y., Maki, T., Washida, K., Kitamura, A., Hase, Y., Ito, H., Takao, K., Miyakawa, T., Kalaria, R.N., Tomimoto, H., Takahashi, R., 2011. The influence of chronic cerebral hypoperfusion on cognitive function and amyloid beta metabolism in APP overexpressing mice. PLoS One 6, e16567.

Yamauchi, H., Kudoh, T., Kishibe, Y., Iwasaki, J., Kagawa, S., 2007. Selective neuronal damage and chronic hemodynamic cerebral ischemia. Ann. Neurol. 61, 454–465.

Yamauchi, H., Higashi, T., Kagawa, S., Nishii, R., Kudo, T., Sugimoto, K., Okazawa, H., Fukuyama, H., 2012. Is misery perfusion still a predictor of stroke in symptomatic major cerebral artery disease? Brain 135, 2515–2526.

Yamauchi, H., Kagawa, S., Takahashi, M., Higashi, T., 2018. Long-term hemodynamic changes and blood pressure in atherosclerotic major cerebral artery disease. J. Cereb. Blood Flow Metab. 2018https://doi.org/10.1177/0271678X17727385. (Epub ahead of print).

Yarchoan, M., Xie, S.X., Kling, M.A., Toledo, J.B., Wolk, D.A., Lee, E.B., Van Deerlin, V., Lee, V.M., Trojanowski, J.Q., Arnold, S.E., 2012. Cerebrovascular atherosclerosis correlates with Alzheimer pathology in neurodegenerative dementias. Brain 135, 3749–3756.

Zetterberg, H., Mortberg, E., Song, L., Chang, L., Provuncher, G.K., Patel, P.P., Ferrell, E., Fournier, D.R., Kan, C.W., Campbell, T.G., Meyer, R., Rivnak, A.J., Pink, B.A., Minnehan, K.A., Piech, T., Rissin, D.M., Duffy, D.C., Rubertsson, S., Wilson, D.H., Blennow, K., 2011. Hypoxia due to cardiac arrest induces a time-dependent increase in serum amyloid beta levels in humans. PLoS One 6, e28263.

Zhang, X., Zhou, K., Wang, R., Cui, J., Lipton, S.A., Liao, F.F., Xu, H., Zhang, Y.W., 2007. Hypoxia-inducible factor 1alpha (HIF-1alpha)-mediated hypoxia increases BACE1 expression and beta-amyloid generation. J. Biol. Chem. 282, 10873–10880.

Zhiyou, C., Yong, Y., Shanquan, S., Jun, Z., Liangguo, H., Ling, Y., Jieying, L., 2009. Upregulation of BACE1 and beta-amyloid protein mediated by chronic cerebral hypoperfusion contributes to cognitive impairment and pathogenesis of Alzheimer's disease. Neurochem. Res. 34, 1226–1235.

Zlokovic, B.V., 2011. Neurovascular pathways to neurodegeneration in Alzheimer's disease and other disorders. Nat. Rev. Neurosci. 12, 723–738.